Int. J. Electrochem. Sci., 10 **(2015)** 1305 - 1315

International Journal of
ELECTROCHEMICAL
SCIENCE
www.electrochemsci.org

Coulometric Titration of Micro-and Nanocrystalline Silver Sulfide

Tadios Tesfu-Zeru

AIT Austrian Institute of Technology GmbH, Giefinggasse 2 | 1210 Vienna | Austria
*E-mail: Tadios.Tesfu-Zeru@ait.ac.at

Received: 27 October 2014 / *Accepted:* 5 December 2014 / *Published:* 16 December 2014

Using coulometric titration, the nonstoichiometry of micro- and nanocrystalline α-$Ag_{2+\delta}S$ (low-temperature phase) is studied as a function of particle size and temperature. The samples are prepared by mechanical ball milling and by precipitation using reverse micelles to obtain particles with narrow size distribution. The nonstoichiometry, the thermodynamic factor, the energy for the formation of electron-hole defects and the concentration of the quasi-free electrons are computed, and the electronic conductivity is measured.

Keywords: coulometric titration, defect chemistry, nanocrystalline, silver sulfide.

1. INTRODUCTION

A considerable interest in the study of the wide homogeneity range of mixed conductors such as silver sulfide is due to their possible applications as heterogeneous catalysts, storage devices and their potential in energy conversion. Silver sulfide has a preponderant electronic and super ionic conductivity, due to the random distribution of Ag^+-ions in the crystal lattice of the material. In 1953, Carl Wagner made the first investigation of the conduction mechanism and introduced coulometric titration to analyze nonstoichiometry of the bulkier Ag_2S [1]. Thereafter the defect chemistry and transport properties of single and polycrystalline Ag_2S at different temperatures were studied.

It has been shown that the enhancement of interface impacts the physical and chemical properties of nanomaterials in comparison to bulk materials. Nanomaterials exhibit fast transport properties due to the novel and short reaction pathways that lead to new modes for the transport of charge, mass, and chemical or energy transformation processes [2]. They possess enhanced surface reactivity due to the higher number of surface atoms with unsatisfied bonds in comparison to the bulk material. The high surface free energy and large surface defects of nanomaterials affect their chemical reactivity, phase stability, and structural transformations, which in turn influence the electrochemical

and catalytic activities of materials. Such phenomena associated with size have been observed in TiO_2, Al_2O_3, nano-Fe_2O_3 and nano-CeO_2 systems [2, 3]. Nanomaterials have significantly enhanced mechanical strength and structural integrity. The underlying mechanisms for their mechanical robustness are yet to be fully investigated [4–7]. Some of the disadvantages of nanostructured materials are the high production cost and undesired side reactions, such as the formation of agglomerates. Recently it has also been shown that a nano-particulate catalyst of a polymer electrolyte membrane (PEM) fuel cell suffers from thermodynamic instability under electric field [8].

The latest reviews [2, 9] highlight the remaining challenges, opportunities, in situ characterization techniques and the major roles of reactive nanomaterials for Li ion and Li air batteries. Generally, a better understanding of electrochemical properties of nanomaterials can be exploited for a new direction in designing new tailor-made energy storage electrode materials. This can offer significant performance improvements in both fuel cell and Li-battery applications.

So far the characterization of the nonstoichiometry (δ) of nanomaterials by coulometric titration has only been performed by the group of Tuller et al. [10]. They showed that the enhancement of nonstoichiometry (phase width) δ of nano $CeO_{2-\delta}$ (particle size of 10 nm $\delta = 10^{-3}$ to 10^{-4}) in comparison to the bulk $CeO_{2-\delta}$ ($\delta = 10^{-9}$) at the temperature of 455 °C and the partial oxygen pressure P_{O2} of 0.21×10^{-5} bars was much larger than expected by Chiang [11] and that δ is proportional to $P_{O_2}^{-1/2}$, while the electron conductivity σ_e was proportional to $P_{O_2}^{-1/6}$. The activation energy obtained from the electron conductivity measurement and the standard enthalpy of defect formation of nano- $CeO_{2-\delta}$ were lower at 1.3 eV and 2.4 eV, respectively, in comparison to the bulk material [12].

The theoretical background and technical applications of coulometric titration are given in [13-16]. This paper focuses on the introduction and discussion of the empirical results of coulometric titration of the micro- and nanocrystalline low temperature silver sulfide material, fabricated by techniques mentioned above.

2. EXPERIMENTAL

2.1. Synthesis of micro- and nanocrystalline Ag_2S

α-Ag_2S was prepared by one-dimensional growth from the elements (sulfur from Merck, 99.9%, and silver rod from Fluka, 99.99%) in a glass tube at a temperature of about 400°C. A cylindrical coarse-grained Ag_2S rod (length = 2 cm and width = 0.5 cm) was obtained with an average growth rate of ca. 10 mm/day. During cooling to room temperature, the transformation from the β-phase (cubic) to the low temperature α-phase (monoclinic) takes place at 176 °C. In order to adjust a defined silver activity, the crystal was equilibrated with a silver metal rod at 100 °C for three weeks. At high temperatures there are tremendous defects that originate from the phase transformation of the high temperature β-$Ag_{2+\delta}S$ to the low temperature α-$Ag_{2+\delta}S$. This is normally accompanied by a significant change of the density of the material [17]. Finally, nanocrystalline α-Ag_2S particles were produced by mechanical ball milling.

Alternatively, monodispersed nanocrystalline α-Ag_2S particles were prepared by using a reverse micelle technique. $6.2x10^{-3}$ g of Na_2S and $42.3x10^{-2}$ g of Ag (AOT) were added to 2 beakers filled with a solution of the surfactant (0.1M Na(AOT) in 100 ml heptane and 9 ml distilled H_2O). The contents of these two beakers were mixed together by stirring. The nanocrystalline Ag_2S was then stabilized using 1μl dodecanethiol per 1ml of the solution. The nanocrystalline α-Ag_2S prepared by the reverse micelle technique was characterized by TEM, and monodisperse nanoparticles with an average particle size of 2.6 nm were found. Note, that the nanoparticles were stabilized by dodecanethiol, which later had a negative impact on the electric conductivity of the compacted material. The characterization of the size distribution of nano α-Ag_2S particles produced by mechanical ball milling was performed by SEM and X-ray diffraction (XRD). The estimation of the average crystallite size using Scherrer´s equation- assuming spherical particles- resulted in average particle sizes of 3μm and 28.1 nm, respectively.

2.2. Coulometric titration setup

A tube furnace with a temperature control of ±1°C was used for heating. The coulometric titration was performed using a Jaissle Model 1000T-B potentiostat. A Keithley 2000 voltmeter was used to measure the electromotive force (emf) E (δ, T). For coulometric titration, the different silver sulfide powders were pressed to pellets of 1 cm diameter and 3 mm thickness. Coulometric titration was performed within a solid state galvanic cell as shown in Eq. (1). Silver could be added to or removed from the silver sulfide sample in order change the deviation δ from stoichiometry of the α-$Ag_{2+\delta}S$ specimen. The solid electrolyte $RbAg_4I_5$ is a pure Ag^+ ion conductor (0.25 S/cm at 25°C) at low temperatures. Between the silver and the $RbAg_4I_5$ a thin layer of a two-phase mixture of silver and $RbAg_4I_5$ was formed which increased the exchange current density of the silver electrode interface, and which improved the stability of the electromotive force E (δ, T) [17].

$$Ag|RbAg_4I_5|\ Ag_{2+\delta}S|\ Pt \qquad (1)$$

Silver removal from α-$Ag_{2+\delta}S$ specimen was always performed at 200 °C, where silver sulfide shows sufficiently high silver mobility. Titration of the α-$Ag_{2+\delta}S$ specimen was performed at 73°C and 150°C, below the phase transformation temperature (176°C). Removing silver out of the α-$Ag_{2+\delta}S$ specimen was done under potentiostatic mode up to E (δ, T) = 0.2 V. Higher emf´s lead to the decomposition of α-$Ag_{2+\delta}S$ by loss of sulfur. Silver was added stepwise into the α-$Ag_{2+\delta}S$ specimen in galvanostatic mode until the α-$Ag_{2+\delta}S$ specimen was in equilibrium with silver at E (δ, T) = 0 V. The titration current I, time t and the electromotive force E (δ, T) were recorded after each step of adding silver into the α-$Ag_{2+\delta}S$ specimen. Fig. 1 presents a sketch of the experimental setup used for coulometric titration.

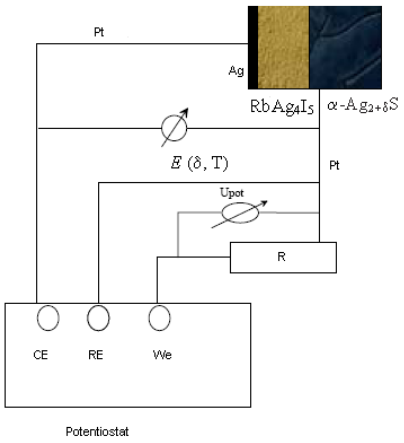

Figure 1. Experimental setup for coulometric titration.

2.3. Electronic conductivity

The electronic conductivity of the pressed silver sulfide pellets was determined in an experimental setup as shown in Fig. 2 by a two-electrode DC measurement. To achieve good contact of the specimen with both platinum electrodes, the surface of the silver sulfide pellet was brushed with platinum paste and pressed between the platinum electrodes. The specific conductivity of the specimen was calculated by assuming negligible interface resistance and negligible ionic conductivity as

$$\sigma_e = 1/\rho = d/(R_{\text{cell}} \cdot A) \qquad (2)$$

where ρ, A and d are the specific resistance (resistivity), cross section area and the thickness of the specimen, respectively.

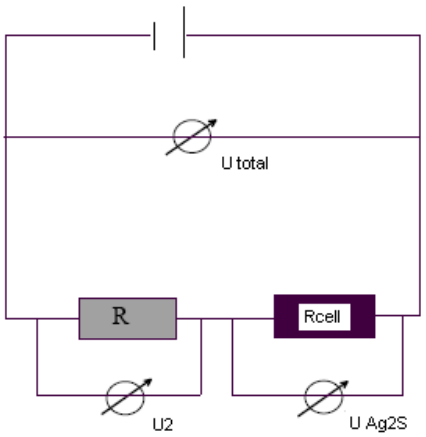

Figure 2. Experimental setup for the electron conductivity measurement of silver sulfide.

3. RESULTS

3.1. Coulometric titration of α-$Ag_{2+\delta}S$

The change in silver excess, i.e. the nonstoichiometry change Δδ achieved by a galvanostatic step, has been calculated by equation (3):

$$\Delta\delta = \frac{V_m}{z\,F\,V_{Ag_2S}} \int I \cdot t \qquad (3)$$

with I, t, V_m, V_{Ag2S} and F as the constant titration current, titration time, the molar volume of silver sulfide (34 cm^3 mol^{-1}), the volume of the specimen and the Faraday constant (96485 C mol^{-1}), respectively.

The electromotive force E (δ, T) of the galvanic cell is in equilibrium directly related to the silver activity a_{Ag} in α-$Ag_{2+\delta}S$ specimen:

$$E(\delta,T) = \frac{(\mu^*_{Ag} - \mu_{Ag})}{F} = -\frac{RT}{F}\ln a_{Ag} \qquad (4)$$

where μ^*_{Ag}, μ_{Ag}, a_{Ag}, T and R denote the chemical potential of pure silver metal as reference, the chemical potential of silver in α-$Ag_{2+\delta}S$, the silver activity in silver sulfide, and the absolute temperature and gas constant, respectively. According to Korte [18] the relation between electromotive force E (δ, T) and the silver excess δ in α-$Ag_{2+\delta}S$ can be determined from its defect thermodynamics.

A typical coulometric titration curve was obtained by plotting E (δ, T) vs. Δδ and fitting it with the arc hyperbolic sine $y = \ln(x + \sqrt{x^2+1})$. The results extracted by fitting the titration curve are the absolute nonstoichiometry δ, the electromotive force E^* (T) at the stoichiometric point, the equilibrium constant K_e for the electron-hole formation, and the Frenkel constant K_f [17, 18].

According to the activity of sulfur (a_s= 1 and a_{Ag} = 0.01) and silver (a_{Ag}= 1 and a_s = 0.001) at equilibrium with silver sulfide at 300 °C, small changes of silver concentration can dramatically change the activity of silver in the specimen [19]. Although the concentration of silver excess (δ = 2.5×10^{-3} at 300°C) is minimal, its influence on the activity of silver in the specimen can be quite significant. This in turn has an impact on the electromotive force E (δ, T) of the solid state galvanic cell according to equation (4).

In Figure 3 representative titration results showing E (δ, T) vs. time under galvanostatic mode at 150°C of silver addition in micro- and nanocrystalline α-$Ag_{2+\delta}S$ specimen are given. The titration started at E (δ, T) = 0.2 V (where silver sulfide is in equilibrium with sulfur) and ended at E (δ, T) = 0 V (where silver sulfide is in equilibrium with silver). As shown in Figure 3, the total titration time of nanocrystalline silver sulfide (275 min) was much longer than for the microcrystalline silver sulfide (100 min), and the decay of E (δ, T) during the titration of the nanocrystalline-specimen is shallower than that of the microcrystalline material. This has come to state, due to the coating of the nanocrystalline by dodecanethiol, which forms strong bonding to stabilize the nanocrystalline particles during the synthesis of the 2.6 nm sized silver sulfide by reverse micelle technique. To achieve equilibrium after each titration step, a waiting time of 5 and 15 minutes for micro- and nanocrystalline samples was chosen.

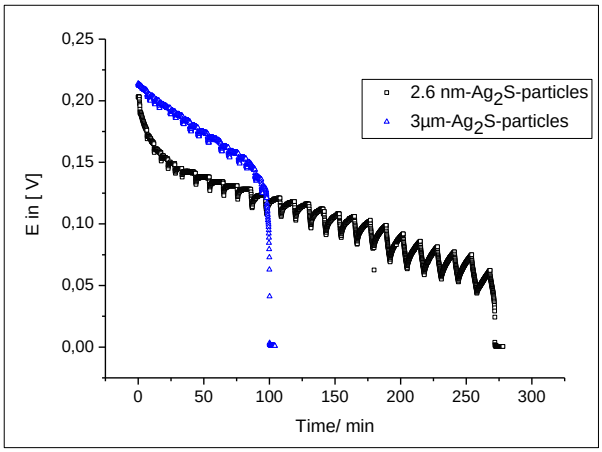

Figure 3. *E* (δ, T) vs. time during coulometric titration of nano- and micro-sized α-$Ag_{2+\delta}S$

Fig. 4 shows coulometric titration curves of nano- and micro-crystalline α-$Ag_{2+\delta}S$ recorded at a temperature of 150 °C. The results clearly show that the phase width decreases with the particle size. The phase width of the particles obtained by the inverse micelle technique (2.6 nm) is much larger than the phase width of ball-milled material (3 µm).

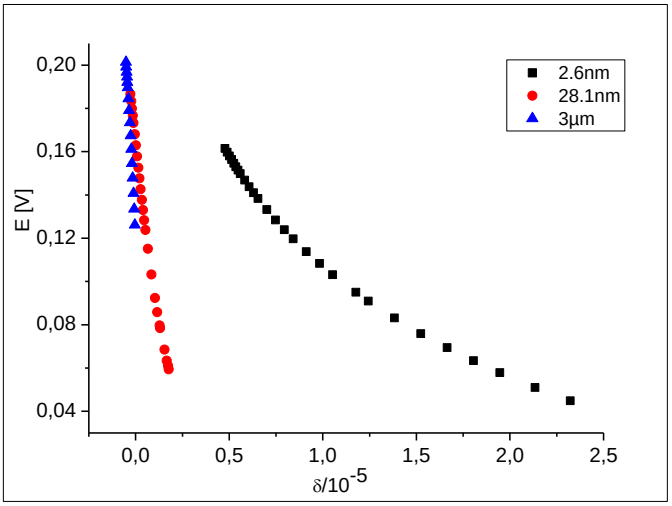

Figure 4. Coulometric titration results of micro-and nanocrystalline $Ag_{2+\delta}S$ at 150 °C.

Fig. 5 shows the titration curves of micro- and nanocrystalline α-$Ag_{2+\delta}S$ produced by mechanical ball milling and measured at temperatures of 73 °C and 157 °C, respectively. Whereas the titration curve of the microcrystalline material changes only slightly with temperature, the titration curve of the nanocrystalline material changes significantly with temperature.

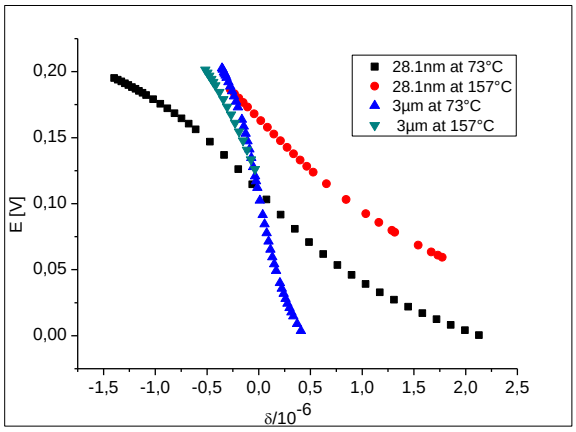

Figure 5. Titration curves of micro- and nanocrystalline α-Ag_2S at different temperatures.

As seen in Figure 5, the titration curves for the nanocrystalline samples become wider and span a larger range of composition. From the coulometric titration curve we can evaluate the thermodynamic factor ($dlna_{Ag}/dlnc_{Ag}$), which is the slope line of the titration curve, and which shows a maximum at the stoichiometric point (δ = 0) [21]:

$$\left(\frac{d\ln a_{Ag}}{d\ln c_{Ag}}\right)_T = -\frac{2F}{RT}\left(\frac{dE}{d\delta}\right)_T \qquad (5)$$

In Fig. 6 a plot of the thermodynamic factor ($dlna_{Ag}/dlnc_{Ag}$) versus nonstoichiometry δ of 3µm and 28.1 nm silver sulfide particles at 73°C and 157°C is shown. As expected, the nanocrystalline samples show a broad and relatively flat curve for the thermodynamic factor.

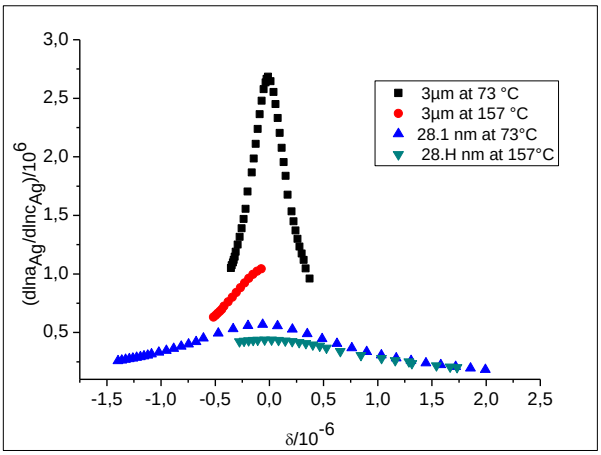

Figure 6. The thermodynamic factor versus the nonstoichiometry δ of micro- and nanocrystalline silver sulfide at 73°C and 157°C.

Using the titration data we have also evaluated the equilibrium constant K_e for the formation of electron-hole pairs. According to the Van't Hoff equation (6) the temperature dependence of K_e is related to the reaction enthalpy $\Delta H°_e$ for the formation of the electron-hole defects.

$$\frac{\Delta H_e^\circ}{RT^2} = \left(\frac{\partial \ln K_e}{\partial T} \right)_{p,x_{e^-}} \qquad (6)$$

Fig. 7 shows a graph of ln K_e versus 1/T [K]. From the slope of the graph, $\Delta H°_e$ of 28.1 nm sized Ag_2S (3.7 kJmol^{-1}) is calculated. This value is considerably smaller than the 100 kJ mol^{-1} value for bulk-Ag_2S reported by Korte [16]. The data are insufficient and can therefore not be fitted reasonably.

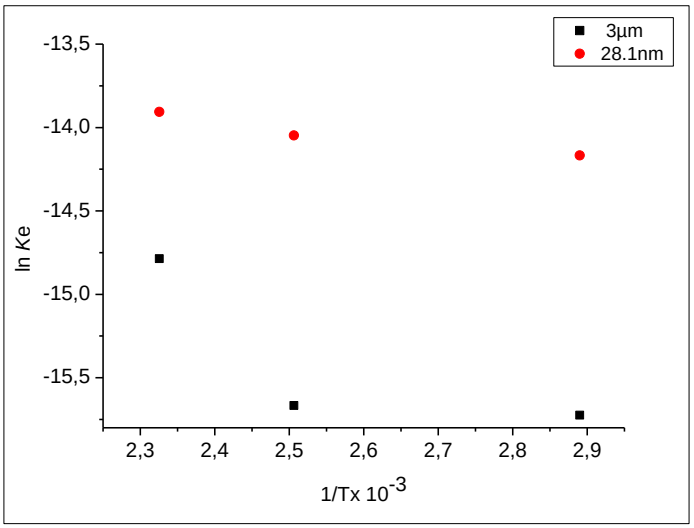

Figure 7. From the slope of ln K_e vs. 1/T [K] the $\Delta H°_e$ can be determined.

To estimate the charge storage capacity and the conductivity of the samples, the concentration of the quasi-free electrons of the sample was calculated. According to Rickert [19], equation (7) can be used to calculate the concentration $n^\bullet$ of quasi-free electrons, assuming that the concentration of electron holes can be neglected. This can be realized when the silver sulfide sample with defined length and volume is at equilibrium with a silver electrode. In this case the silver sulfide sample is enriched with silver. Therefore the chemical potential of silver μ_{Ag} in the sample and silver metal is the same and E (δ, T) = 0. In table 1 the concentrations of quasi-free electrons of 3 µm and 2.6 nm sized Ag_2S particles as function of temperature and $\delta^\bullet$ are presented.

$$n^\bullet \approx \frac{L}{V_m} \delta^\bullet \qquad (7)$$

where: $n^{\bullet}$ cm^{-3} is the quasi-free electron concentration, $\delta^{\bullet}$ the nonstoichiometry of silver sulfide, in which silver sulfide is at equilibrium with silver metal (E (δ, T) = 0), V_m volume and L the length of the specimen, respectively.

The concentration of the quasi-free electrons n• cm^{-3} is increased and decreased with temperature and particle size, respectively.

Table 1. The computed concentration of quasi-free electrons $n^{\bullet}$ cm^{-3} as the function of particle size and temperature in which silver sulfide sample is at equilibrium with silver $\delta^{\bullet}$.

3 μm sized Ag_2S	$\delta^{\bullet}$	$n^{\bullet}$[cm^{-3}] at $\delta^{\bullet}$
73 °C	$4.08 \cdot 10^{-7}$	$3.22 \cdot 10^{19}$
126 °C	$6.96 \cdot 10^{-7}$	$5.49 \cdot 10^{19}$
2.6 nm sized Ag_2S		
73 °C	$2.51 \cdot 10^{-6}$	$1.99 \cdot 10^{20}$
126 °C	$3.06 \cdot 10^{-4}$	$2.42 \cdot 10^{22}$

3.2. Results of electron conductivity measurements

Table 2. Electron conductivity of micro- and nanocrystalline silver sulfide as the function of particle size and temperature.

Temperature/°C	σ_e/Scm^{-1} of 3μm sized Ag_2S	σ_e/Scm^{-1} of 28.1 nm sized Ag_2S	σ_e/Scm^{-1} of 2.6 nm sized Ag_2S
73 °C	$2.64 \cdot 10^{-2}$	$3.66 \cdot 10^{-2}$	$3.30 \cdot 10^{-3}$
126 °C	$4.59 \cdot 10^{-2}$	$8.40 \cdot 10^{-2}$	$2.57 \cdot 10^{-2}$
150 °C	$5.46 \cdot 10^{-2}$	$9.24 \cdot 10^{-2}$	$6.40 \cdot 10^{-2}$

Table 2 presents the results for the electronic conductivity of silver sulfide at different temperatures and particle sizes. Notice that the three samples investigated here were prepared by different techniques (see part 2.1.). Nanocrystallines of 3μm and 28.6 nm sized α-Ag_2S were prepared from their elements at high temperature and atomized from bulk to micro-and nanocrystalline by mechanical ball milling. These two samples were free of any organic coatings. Vice versa, the 2.6 nm sized nanocrystalline α-Ag_2S were prepared by the reverse micelle technique and stabilized using dodecanethiol. Due to a large surface area and high grain boundaries of nanocrystalline materials, a much higher electron conductivity from the 2.6 nm sized silver sulfide than microcrystalline silver sulfide is expected. Unfortunately, the electron conductivity of the 2.6 nm sized silver sulfide was comparable to the other two samples. The mismatch of the theoretical expectation and experimental

result can be explained by the fact that the 2.6 nm sized silver sulfide were coated by dodecanethiol, which adversely affected the conductivity of the sample.

4. DISCUSSION

Two different synthesis techniques were used to control the particle size distribution of silver sulfide material. The α-Ag_2S were prepared at high temperature from its elements and afterwards downsized from bulk to 3µm and 28.6 nm by mechanical ball milling. The 2.6 nm sized silver sulfide particles were prepared by using a reverse micelle technique during a reaction of sodium sulfide with Ag (AOT) in an emulation of heptane, H_2O and surfactant. The obtained nanocrystalline Ag_2S were then stabilized using 1µl dodecanethiol per 1ml of the solution.

Using coulometric titration, the nonstoichiometry of micro- and nanocrystalline α-$Ag_{2+\delta}S$ were studied as a function of particle size and temperature. Additionally, the electron conductivity of the samples was measured to compare the size effect on their electrochemical properties. The nonstoichiometry, the thermodynamic factor, the energy for the formation of electron-hole defects and the concentration of the quasi-free electrons were calculated or obtained from the results of the coulometric titration data.

The results of coulometric titration of silver sulfide as a function of their particle size and temperature indicated that some of the specimens show an enhancement or broadness of the nonstoichiometry dependent on their particle size and temperature. The maximum of the thermodynamic factor decreased with increasing temperature and decreasing particle size. The standard reaction enthalpy decreased with downsizing of the particle size.

The enhancement of the electronic conductivity as a function of the particle size and temperature, as found in the relevant literature, was verified. The enhancement of the electronic conductivity with decreasing particle size was observed. Nevertheless, the poor electron conductivity of the 2.6 nm sized silver sulfide can be explained by the stable strong bonding of the nanoparticles with dodecanethiol, which was used to stabilize the nanoparticles after synthesis.

5. CONCLUSIONS

We succeeded in applying the coulometric titration technique to samples prepared from stabilized nanoparticles. The time for equilibration of the nanoparticle-based samples increases compared to microcrystalline samples, indicating the huge surface area and the enhanced grain boundaries in the nanocrystalline in comparison to the bulk, which can be used as charge storage sites in this material. The phase width of the nanocrystalline samples has increased considerably compared to microcrystalline material. The analysis of the results shows that the energy for the formation of electron hole-pairs has decreased massively for the nanoparticle-based samples.

References

1. C. Wagner; *J. Chem. Phys*. 21(1953) 1819.
2. M.-K. Song, *Mater. Sci. Eng*. R 72 (2011) 203.
3. M. Fernandez-Garcia, A. Martinez-Arias, J.C. Hanson, J.A. Rodriguez, *Chem. Rev*. 104 (2004) 4063–4104.
4. H. Gleiter, *Prog. Mater. Sci*. 33 (1989) 223–315.
5. K.S. Kumar, H. Van Swygenhoven, S. Suresh, *Acta Mater*. 51 (2003) 5743–5774.
6. M.A. Meyers, A. Mishra, D.J. Benson, *Prog. Mater. Sci*. 51 (2006) 427–556.
7. G. He, J. Eckert, W. Loser, L. Schultz, *Nat. Mater*. 2 (2003) 33–37.
8. R. Borup, et al., *Chem. Rev*. 107(2007) 3904–3951.
9. Kyu Tae Lee, Jaephil Cho, www.elsevier.com/locate/nanotoday (2011).
10. H. L. Tuller, O. Porat, E. B. Lavik, Y.M. Chiang, *Mat. Res. Soc. Symp. Proc*., 457 (1997).
11. Y. M. Chiang, E. B. Lovik, I. Kosucki, H. L. Tuller, J. Y. Ying, *J. Appl. Phys. Lett*. 69 (1996) 185.
12. H. L. Tuller, A. S. Nowick, *J. Electrochem. Soc*. 126 (1979) 209.
13. T. Tesfu-Zeru, Ph.D. Thesis, University of Giessen/Germany (2004).
14. H. Schmalzried, *prog. solid st. chem*., 13 (1980) 119-157.
15. D. Grientschnig and W. Sitte; *J. phys. solids*, Vol. 52, No. 6 (1991) 805-820.
16. C. Korte, Ph.D. Thesis, University of Hannover (1997).
17. G. Beck, J. Janek, *Physica*, B 308-310 (2001) 1086.
18. C. Korte, J. Janek, *Z. Phys. Chem*. 206 (1998) 129.
19. H. Rickert, Electrochemistry of Solids, Springer Verlag, Berlin 1982C.
20. T. Best, diploma thesis, University of Giessen (12/2001).
21. C. Wagner, Atom Movements, ASM, Cleveland (1951), p. 153. 17
22. L.S. Darken, *Trans. AIME* 178 (1948) 184.
23. J. Maier, *Prog. Solid State Chem*. 23 (1995) 171.
24. S. Indris, Ph.D. Thesis, University of Hannover, 65 (2001).